Astron. Astrophys. 335, L73–L76 (1998)

ASTRONOMY AND ASTROPHYSICS

LETTER

*Letter to the Editor*

# The role of the f-mode in the relation between solar intensity oscillations and granulation

**M. Kiefer**[1] **and H. Balthasar**[2]

[1] Kiepenheuer-Institut für Sonnenphysik, Schöneckstrasse 6, D-79104 Freiburg, Germany (e-mail: kiefer@kis.uni-freiburg.de)
[2] Astrophysikalisches Institut Potsdam, Telegrafenberg, D-14473 Potsdam, Germany (e-mail: hbalthasar@aip.de)

Received 23 February 1998 / Accepted 22 May 1998

**Abstract.** A series of white-light images is used to examine the relation of solar intensity oscillations and the granulation structure. Much of the oscillation power lies on the f-mode ridge in the diagnostic diagram. Filters are constructed to separate granulation, $p$-modes, and the f-mode. The filtered data are used to investigate the relation between rms-amplitudes of the oscillations and the granulation structure. Both $p$-modes and f-mode show a tendency to increased amplitudes in the darkest features of the granulation structure, with the f-mode showing this preference for dark regions much clearer. We emphasize that due to the different propagation characteristics of $p$-modes and the f-mode a separation like ours is mandatory to draw conclusions about wave excitation and diffraction.

**Key words:** Sun: granulation – Sun: oscillations

## 1. Introduction

In recent years much attention has been paid to the question, whether the structure of convection, and especially the granulation structure visible in the photosphere, has some influence on the excitation and propagation of waves in the Sun.

Using data of Doppler velocity in several heights in the photosphere, Rimmele et al. (1995) find acoustic events to be located preferentially in intergranular lanes. They get a time delay between the further darkening of an already dark structure and the onset of the acoustic event of typically 1–2 minutes.

Espagnet et al. (1996) used intensity and velocity data to examine the relation between oscillations and the granulation structure. They separated oscillations and granulation by filtering in the $k-\nu$ space and find that intensity oscillations, dominated by cells with sizes of $2''$–$3''$, prefer dark locations in the granulation. Applying statistical methods they further find that velocity oscillations also tend to prefer dark regions.

Hoekzema et al. (1998) used intensity data to examine the relation between oscillations and granulation structure. They filtered the data in the spatial and temporal domains. For oscillation frequencies $\nu > 4$ mHz they find a preference for dark regions which strengthens with increasing frequency. No evidence for increased oscillation amplitudes of waves in the period range of 5 min is found for dark regions.

There are essentially two theoretical approaches connected to the observed features. The first one is the model of localized wave excitation (Brown 1991) in connection with the role of developing downdrafts as generators of acoustic noise (e.g. Rast 1997). The second one is based on the diffraction of sound waves propagating through an inhomogeneous medium (Zhugzhda & Stix 1994 and Stix & Zhugzhda 1996).

The differences of the $p$-modes and the f-mode with respect to their physical and propagation properties must not be underestimated when drawing conclusions from the behavior of evanescent waves alone. In the photosphere and below the $p$-modes, due to their oblique propagation direction, will "see" quite a different structure than the horizontally propagating f-mode. A separation of the two wave types therefore seems to be highly advisable for any analyses concerned with the relation between solar oscillations and granulation. In contrast to previous approaches we use filters to separate $p$-modes and the f-mode in the data.

## 2. Observation and data processing

The data were taken on July 6, 1996 at the German VTT at the Observatorio del Teide, Tenerife. A field of $76'' \times 55''$ of magnetically quiet Sun at disc center was observed for 119 min with the CCD1-camera of the 2D-spectrometer of the Göttingen University (Bendlin & Volkmer 1995). The pixel size corresponds to $0\farcs2 \times 0\farcs2$. The initial data consisted of 160 temporal equidistant blocks of 40 images each. The recording of the 40 images took 11 s, the time from block to block was 44.8 s, each image was exposed for $3 \times 20$ ms. We used a filter centered at 709 nm with a FWHM of 0.3 nm. The seeing conditions varied from moderate to good during the observation.

Standard procedures like dark current and gain table corrections were performed. Image motion and distortion were removed by means of correlation analysis and by applying a destretch algorithm. The algorithm only corrects for geometric,

*Send offprint requests to*: M. Kiefer

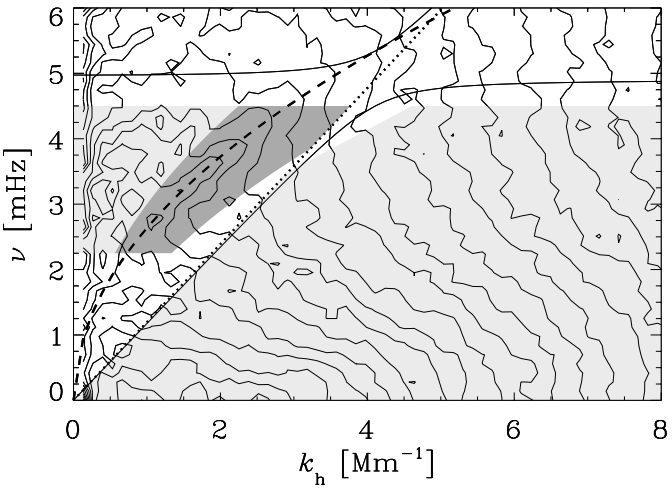


**Fig. 1.** Power of series A in the diagnostic diagram. Isocontours are separated by a factor of $\sqrt{10}$. Dotted line: Lamb-mode with $\nu = \frac{1}{2\pi} c_{\rm s} k_{\rm h}$, heavy broken line: dispersion relation for surface waves, $\nu = \frac{1}{2\pi}\sqrt{g k_{\rm h}}$ ($c_{\rm s} = 7.5$ km/s, $g = 274$ m/s$^2$). Light shading outlines the areas of the filters for $p$-modes (left) and granulation (right) and medium shading shows the region of the f-mode filter.

but not for photometric effects of image distortions. After all corrections the image size was reduced to $65'' \times 43''$. For the subsequent analyses two series were extracted from the $160 \times 40$ images: The first, *series A*, is composed of 160 averaged images of the respective blocks of 40. The second, *series B*, consists of the respective best image of each block of 40, which gives a series of 160 images, not perfectly equidistant in time. The reason for this separation is: the best images show the granulation structure with sufficient quality and the images of series A are less contaminated by the intensity artifacts introduced by the destretching due to the averaging process.

## 3. Power in the diagnostic diagram and filtering

Prior to all of the following procedures a linear fit was subtracted from each single image. For calculating the power spectra of our data we used a Hanning window. Assuming horizontally isotropic conditions on the Sun allows the reduction of three-dimensional Fourier data to the two-dimensional diagnostic diagram by integrating on circles with constant horizontal wavenumber, $k_{\rm h}$, in the $k-\nu$ space.

Fig. 1 shows the power of series A in a logarithmic scaling in the diagnostic diagram. The most prominent feature in the oscillation range is the ridge belonging to the dispersion relation for surface waves, which correspond to the f-mode for global coherent waves. Note that only nonadiabatic surface waves with the dispersion relation $\nu = \frac{1}{2\pi}\sqrt{g k_{\rm h}}$ cause intensity fluctuations (Zhughzda 1991). The ridge is clearly discernible to wavenumbers of 3 Mm$^{-1}$ which corresponds to an oscillation degree $l = 2100$ or a wavelength of $2''.9$. There is a weak indication for a further ridge to the left of the f-mode which might correspond to the $p_1$-mode. In general the $p$-modes do not show up clearly in our data. To quantify the power distribution we give some values below.

The features in the diagnostic diagram guided the construction of filters to separate the diverse phenomena in the data. We defined four basic filters for granulation, $p$-modes, f-mode, and evanescent waves, where the latter is the combination of the $p$-modes and f-mode filters. See Table 1 for a detailed description. For the three oscillation filters we defined "low frequency" and "high frequency" subsets with the frequency ranges 2.25–3.375 mHz and 3.375–4.5 mHz, respectively. Apart from the division line between $p$-modes and f-mode all edges of the filters were smoothed to reduce ringing effects.

The filtered time series were obtained through the following procedure: An apodization was applied to 10% of the data at each border of the two spatial and the temporal domains. After Fourier transformation the data were multiplied by the filter function, transformed back and divided by the apodization function. At each border 5% of the resulting data were cut off which left a data set of spatial dimensions $59'' \times 39''$ and duration 107 min. The granulation filter was applied to the series B, the nine oscillation filters were applied to the series A.

The relative rms values in intensity for the filtered data series are shown in Table 2. Obviously the f-mode is an important contributor to the power in intensity oscillations. Its power almost equals the total power of all $p$-modes which can be detected in our field of view.

## 4. Granulation and oscillations

Similar to Hoekzema et al. (1998) we defined pixel classes based on intensity values to define granulation features. We chose ten intensity classes: In the first class, [0, 0.1], there are the ten percent darkest pixels, in the second class, [0.1, 0.2], there are the pixels for which 10% of all pixels are darker and 80% of all pixels are brighter, and so on.

Each of the granulation images was divided into the aforementioned classes which gave ten respective pixel patterns corresponding to regions of certain intensity ranges. The patterns were then used in the images of each oscillation series to extract oscillation amplitudes which were squared and added up for each image. Within the pixel classes these sums then were summed over all images, which gave ten numbers for each oscillation series. From these ten numbers we first derived ten relative values by dividing through the numbers of pixels of the respective patterns. Secondly all ten numbers were added up and divided by the sum of all numbers of pixels of the patterns. The final results then are the square roots of the relative values divided by the total value. These final values are the area-related ratios between the rms values in certain classes and the total rms value in the corresponding series. Shifting the series of patterns in time with respect to the oscillation images yielded information about a delay in the interaction of oscillations and granulation structure. Fig. 2 shows gray scale images of the rms amplitude ratios for the nine oscillation filters. From top to bottom row there are images for $p$-modes, f-mode, and evanescent waves, respectively. The left column shows results for the ba-

**Table 1.** Definition of the four basic filters in the $k_{\rm h}$-$\nu$ plane (sound velocity $c_{\rm s} = 7.5$ km/s, gravitational acceleration $g = 274$ m/s$^2$).

| | | | | | | | | |
|---|---|---|---|---|---|---|---|---|
| granulation | | $\nu < 4.5\,$mHz | and | $\nu < \frac{1}{2\pi} c_{\rm s} k_{\rm h}$ | and | $\nu < \frac{1}{4\pi} c_{\rm s} k_{\rm h} + 1.75\,$mHz | | |
| $p$-modes | $2.25\ {\rm mHz} < \nu < 4.5\,$mHz | | and | | | $\nu > \frac{1}{2\pi}\sqrt{1.3 g k_{\rm h}}$ | | |
| f-mode | $2.25\ {\rm mHz} < \nu < 4.5\,$mHz | | and | $\nu > \frac{1}{2\pi} c_{\rm s} k_{\rm h}$ | and | $\nu < \frac{1}{2\pi}\sqrt{1.3 g k_{\rm h}}$ | and | $\nu > \frac{1}{2\pi}\sqrt{0.9 g k_{\rm h}} - 0.64\,$mHz |
| evanescent waves | $2.25\ {\rm mHz} < \nu < 4.5\,$mHz | | and | $\nu > \frac{1}{2\pi} c_{\rm s} k_{\rm h}$ | and | | | $\nu > \frac{1}{2\pi}\sqrt{0.9 g k_{\rm h}} - 0.64\,$mHz |

**Table 2.** Relative rms values in percent for the intensity fluctuations of the four filtered time series for the basic filters defined in Table 1 and the respective low and high frequency subsets (2.25–3.375 and 3.375–4.5 mHz).

| type | granulation | $p$-modes | f-mode | evanesc. waves |
|---|---|---|---|---|
| basic | 2.2 | 0.36 | 0.33 | 0.50 |
| low | – | 0.25 | 0.25 | 0.36 |
| high | – | 0.23 | 0.19 | 0.31 |

sic filters as introduced in Table 1, the middle column those for the "low frequency" subsets, and the right column those for the "high frequency" subsets. The abscissa gives the time delay, $\Delta t$, between the oscillation and the pattern series where positive values signify delayed reaction of the oscillations. The ordinate gives the intensity/pixel classes in the notation introduced above.

At first glance there is a clear preference for the very darkest locations of granulation in all oscillation series, although this is a small effect at a level of some percent only. A closer look reveals some interesting differences between the $p$-mode and f-mode behavior. For the $p$-modes (first row of Fig. 2) there is a slight tendency for higher amplitudes to prefer the darkest regions and to avoid the brightest ones. For the high frequencies (right) this tendency is more pronounced and there is a time delay, both for the regions of preference and avoidance, of about 7 min. The low frequencies (middle) show a similar behavior, although on a much lower level. The preference and avoidance behavior of the f-mode with respect to dark and bright regions (second row) is much more pronounced, compared to the $p$-modes. The amplitude ratio reaches 1.08 compared to 1.03 for the $p$-modes. Moreover there is no time delay for high amplitudes with respect to dark regions but a negative delay in the avoidance regions. The high frequency f-mode waves show no clear tendency for avoidance of the brightest regions. The last row of Fig. 2 depicts the behavior of evanescent waves. All three images essentially give the same impression: There is preference of the darkest regions and avoidance of the brightest ones by the oscillations. The time delay is 1–2 min for preference, and 3–5 min for avoidance.

## 5. Discussion and interpretation

Our results with respect to the evanescent waves are consistent with those of Espagnet et al. (1996). Their observed cell sizes of $2''$–$3''$ mean that their "5-min oscillations" probably get strong contributions from the f-mode.

We want to emphasize that the results for evanescent waves are caused by a superposition of $p$-mode and f-mode behavior, where the latter is the dominant one. It is thus not advisable to draw specific conclusions about wave excitation or diffraction from the results for evanescent waves alone. Therefore we examined the $p$-mode and the f-mode oscillations separately. Our interpretation of the quite different behavior of the two wave types is as follows: The preference of the darkest regions is more pronounced for the higher frequency $p$-modes which is consistent with the model proposed by Zhugzhda & Stix (1994) and Stix & Zhugzhda (1996). Here the delay might indicate that when an intergranular region enters the class of the darkest pixels it needs some time to establish a strong coherent downflow which leads to noticeable diffraction of the wave into the channel of cool downstreaming material.

According to Murawski & Roberts (1993) and Rosenthal et al. (1995) f-mode frequencies are affected by convective flows. We propose that horizontal granular flows cause an advective distortion of the wave field which might lead to the observed behavior of the f-mode. Here it is important to recall that the surface waves propagate horizontally and quite rapidly decay in the subphotospheric layers. Therefore the waves might well be influenced by horizontal flows in the photosphere. This view is supported by the fact that the horizontal granular rms velocity reaches 1.5 km/s and more (Title et al. 1989) which can not be neglected in comparison with the f-mode phase velocities of 9–18 km/s in our f-mode filter range. A problem in interpreting the f-mode data is the close vicinity to the region which we defined as granulation in the diagnostic diagram. There might be some misleading cross talk. This problem can not be overcome with data of the continuum intensity alone.

## 6. Conclusions

Our conclusions are as follows:

1. The f-mode is an important contributor to the power of the intensity oscillations in the regime of evanescent waves.
2. The relation between amplitudes of intensity oscillations and granulation structure are quite different for $p$-modes and for the f-mode. The latter dominates the behavior of the evanescent waves.
3. Investigations with respect to the relation between oscillations and granulation structure have to be carried out with an appropriate separation of $p$-modes and the f-mode. This

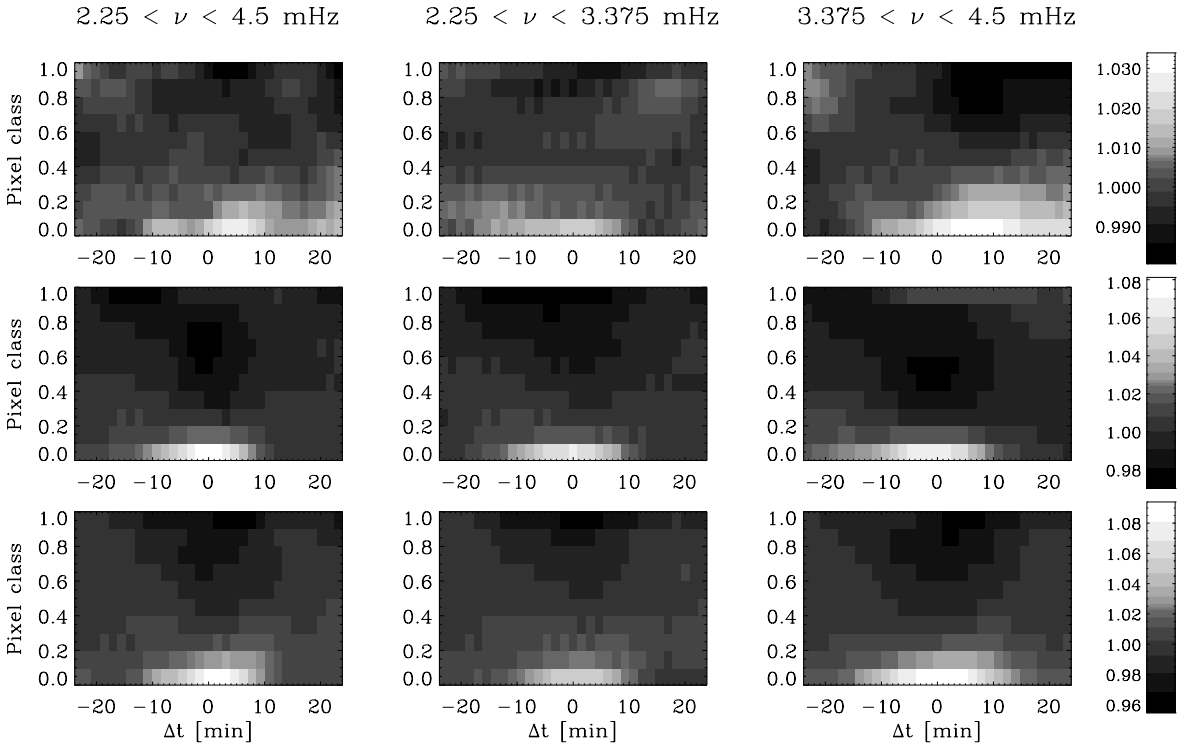


**Fig. 2.** Grayscale plots of the ratio of rms amplitudes in intensity classes to the total rms amplitude for three types of oscillations: $p$-modes (first row), f-mode (second row), and evanescent waves (third row). The abscissa gives the time delay between the series of oscillations and pixel patterns. The ordinate shows the ten intensity/pixel classes. Each row is scaled individually in the range indicated by the bar to the right of it.

is further suggested by the different propagation properties of the two wave types.

4. Any conclusions with respect to either excitation or diffraction of $p$-modes drawn from examination of evanescent intensity oscillations alone are misleading.
5. A better theoretical understanding of the f-mode and its interaction with the convective flow field is necessary.

It is important to note that, even if the f-mode in intensity oscillations was strongly contaminated by crosstalk from the adjacent region of granulation in the $k-\nu$ space, our conclusions remain essentially unchanged. The term "f-mode" then should be changed to "apparent f-mode". This would especially not alter the main conclusion: If one wants to learn something about the relation between solar oscillations and convection/granulation structure, be it about excitation or about propagation in inhomogeneous media, one has to do a careful and suitable filtering of the data. Needless to say that only with the best available 2-D data, preferentially intensity *and* Doppler velocity, there is a chance to arrive at conclusive findings with respect to the questions under consideration.

*Acknowledgements.* We gratefully acknowledge useful discussions with W. Schmidt and M. Stix (KIS) and with J. Staude and Y. Zhugzhda (AIP). The VTT on Tenerife is operated by the Kiepenheuer-Institut für Sonnenphysik (Freiburg) in the Observatorio del Teide of the Instituto de Astrofísica de Canarias. The Göttingen 2D-spectrometer was supported by the *Deutsche Forschungsgemeinschaft*.

## References

Bendlin C., Volkmer R., 1995, A&AS 112, 371
Brown T.M., 1991, ApJ 371, 396
Espagnet O., Muller R., Roudier T., Mein P., Mein N., Malherbe J.M., 1996, A&A 313, 297
Hoekzema N.M., Rutten R.J., Brandt P.N., 1998, A&A 333, 322
Murawski K., Roberts B., 1993, A&A 272, 601
Rast M.P., 1997, in: SCORe'96: Solar Convection and Oscillations and their Relationship, eds. F.P. Pijpers, J. Christensen-Dalsgaard, C.S. Rosenthal Kluwer, Dordrecht, (1997), p.135
Rimmele T.R., Goode P.R., Harold E., Stebbins R.T., 1995, ApJ 444, L119
Rosenthal C.S., Christensen-Dalsgaard J., Nordlund Å., Trampedach R., 1995, in: Proceedings of the 4$^{\rm th}$ SOHO Workshop, esa SP-376, vol. 2 eds. J.T. Hoekzema, V. Domingo, B. Fleck, B. Battrick, p. 453
Stix M., Zhugzhda, Y.D., 1996, in: Cool Stars, Stellar Systems, and the Sun, 9th Cambridge Workshop, PASP Conf. Ser. 109, ed. R. Pallavicini, p.163
Title A.M, Tarbell T.D., Topka K.P., Ferguson, S.H., Shine, R.A., and the SOUP Team, 1989, ApJ 336, 475
Zhugzhda Y.D., Stix M., 1994, A&A 291, 310
Zhugzhda Y.D., 1991, Sol. Phys. 132, 205